Improvements to the Mercury Electric Dipole Moment Experiment

Kyle Matsuda*
Department of Physics, Harvard University, Cambridge, MA 02138

Advisor: Blayne Heckel
Department of Physics, University of Washington, Seattle, WA 98195
(Dated: August 28, 2015)

New systematic effects have been identified in the latest and most sensitive search for the ^{199}Hg electric dipole moment. This project mapped the magnetic field gradients inside of the experimental apparatus as a preliminary effort toward determining the cause of these systematics and bounding their effect on the electric dipole moment measurement.

I. INTRODUCTION

A nonzero permanent electric dipole moment (EDM) of an atom or elementary particle would provide direct evidence for T-violation, and would imply violation of CP-symmetry via the CPT theorem. While the standard model predicts EDM values that are many orders of magnitude smaller than current experimental bounds, many new theories predict much larger values that are within experimental reach. Indeed, current bounds already constrain the parameter space of standard model extensions such as supersymmetry [1].

In 2009, our group published a new bound on the EDM of ^{199}Hg, $d(^{199}\text{Hg}) < 3.1 \times 10^{-29}$ e cm [2]. This result is the most sensitive search for the EDM of a diamagnetic atom to date, and gives improved limits on CP-violation in extensions to the standard model [3].

Recently, our experiment completed a new EDM dataset. Several major improvements to the experiment, including eliminating the dominant source of systematic error from the previous result (leakage currents across the Hg vapor cells), have led to a significant increase in the sensitivity of our measurement. We expect to achieve a factor of 3 to 4 improvement in statistical sensitivity compared to our last published result.

My work this summer focused on determining the cause of a new systematic effect that has appeared in our most recent dataset, which we call the "B-even" effect. To investigate this effect, I built a new translation apparatus to move the Hg vapor cells within the main magnet coil. This has allowed us to map the magnetic field gradients inside of our apparatus and place bounds on the feedthrough of the B-even systematic to our EDM measurement. In addition, this mapping has allowed us to measure how changes in EDM insensitive frequency channels (used for looking for systematics) propagate to the EDM channel; this allows us to place bounds on the feed through of another systematic effect, an anomalously large frequency difference between the outer cells, to our EDM measurement.

* kmatsuda01@college.harvard.edu

Section II gives a brief introduction to the experiment. Section III describes two of the most significant systematic effects that appear in the most recent dataset. My contributions to mapping the magnetic field gradients are discussed in Section IV, and plans for a new magnetic shield are described in Section V; Section VI gives a brief summary.

II. EXPERIMENTAL OVERVIEW

^{199}Hg has a $^1S_0$ electronic ground state and nuclear spin $I = 1/2$. An EDM of the ground state must point along the nuclear spin axis, since this is the only quantum axis in the atom.

The Hamiltonian for spin-polarized ^{199}Hg in parallel or antiparallel magnetic ($\mathbf{B}$) and electric ($\mathbf{E}$) fields is given by $H = -\boldsymbol{\mu}\cdot\mathbf{B} - \mathbf{d}\cdot\mathbf{E}$, where $\boldsymbol{\mu}$ and $\mathbf{d}$ are the magnetic and electric dipole moments of ^{199}Hg. This corresponds to a Larmor frequency of $h\nu = 2|\mu B \pm dE|$, where the $+(-)$ indicates applied fields that are parallel (antiparallel). The signature for a nonzero EDM is a shift $\delta\nu$ in the Larmor frequency when $\mathbf{E}$ is reversed relative to $\mathbf{B}$,

$$\delta\nu = \frac{4dE}{h}. \tag{1}$$

Our experiment uses a stack of four vapor cells which contain isotopically enriched (92%) ^{199}Hg, which are held in a conductive vessel (shown in Fig. 1). The vessel sits inside of the main magnet coil, which is surrounded by three layers of magnetic shielding made of high permeability mu-metal. The cells are placed in a common magnetic field of about 10 mG, which sets the Larmor frequency of the Hg atoms at about 8 Hz. The two middle cells are separated by a ground plane and the two outer cells are enclosed by high voltage (HV) electrodes that are placed at ±6 or 10 kV. Thus, the middle cells experience oppositely directed electric fields, while the outer cells are held at $E = 0$. A schematic of the experiment is shown in Fig. 2.

With this configuration, the difference in the Larmor frequencies of the two middle cells is equal to $\delta\nu$ (ignoring systematic effects) from Eq. 1. The outer cells have no EDM sensitivity, but are used as comagnetometers and are helpful for checking for systematic effects.

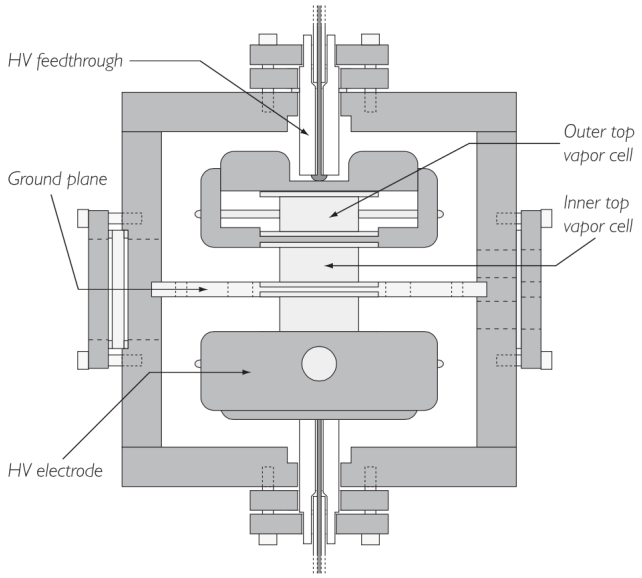

FIG. 1. A drawing of the EDM vessel, from Ref. [3]. Vapor cells are drawn in gray; the outer bottom cell is obscured by the bottom electrode, while the top electrode is cut away to show the outer top cell.

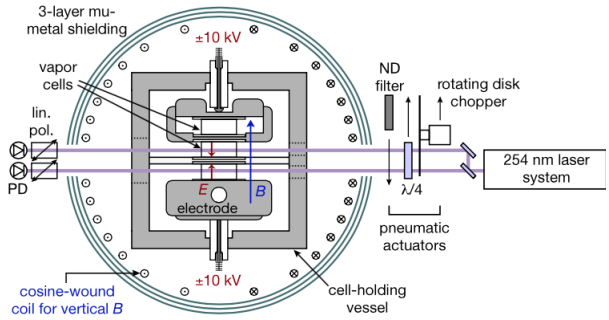

FIG. 2. A schematic of the apparatus, from Ref. [2].

To make our measurement, we first build up spin polarization by optically pumping on the ${}^1S_0(F = 1/2) \rightarrow {}^3P_1(F = 1/2)$ line at 254 nm. About 30 μW of resonant light is directed tranverse to the magnetic field and intensity-modulated at the Larmor frequency with a rotating chopper wheel. This pump phase builds up precessing Hg spin polarization in a plane normal to $\mathbf{B}$. During the probe phase, the light is changed to linear polarization, attenuated to about 3 μW, and detuned from the pump transition. The Hg spin precession about $\mathbf{B}$ causes optical rotation of the probe light; the angle of rotation is measured using a linear polarizer followed by a photodiode. To extract the Larmor frequency for each cell, the photodiode signals during the probe phase are fitted to the form

$$I(t) = A\sin(\omega t + \phi)e^{-\Gamma t} + C. \qquad (2)$$

To extract the EDM signal, the following linear combination of Larmor frequencies is used,

$$\nu_c = \nu_{\mathrm{EDM}} = \nu_{\mathrm{MT}} - \nu_{\mathrm{MB}} - \frac{1}{3}\left(\nu_{\mathrm{OT}} - \nu_{\mathrm{OB}}\right), \qquad (3)$$

where MT refers to the middle top cell, OB refers to the outer bottom cell, etc. The frequency combination ν_c, which we often refer to as the "combo channel" or "EDM channel," is maximally sensitive to frequency shifts due to an EDM while also canceling magnetic field gradient noise in the $\hat{y}$ direction through first and second order.

Greater detail on the experiment is given in Ref. [3]. However, several improvements have been made to the apparatus and measurement technique for the most recent dataset. Most relevant to this report, the gold-coated fused silica ground plane was replaced with a quartz ground plane, which has a higher work function. The vessel was also continuously flushed with dry air instead of either SF_6 or N_2. These changes helped to significantly reduce leakage currents and sparks, two of the primary sources of systematic error from the result in Ref. [2], causing the new effects discussed below to emerge as the dominant remaining systematic effects.

III. NEW SYSTEMATIC EFFECTS

A. B-Even Effect

To test for systematic effects, we take EDM measurements with $\mathbf{B}$ pointing in two different directions ($\pm\hat{y}$ in the coordinate system of our apparatus), and with two values of $\mathbf{E}$ (approximately 6 or 10 kV/cm). This gives four distinct field configurations. If we then plot the frequency shift $\Delta\nu_c$ in our combo (EDM) channel against the electric field magnitude relative to the direction of $\mathbf{B}$, we obtain the graph in Fig. 3. Since $\Delta\nu_c \propto dE$, we would expect to see zero frequency shift due to an EDM when $E = 0$. Therefore, the offset seen in Fig. 3 indicates a possible source of systematic error. We call this B-independent offset the "B-even effect," since it seems to imply that some portion of our signal does not reverse when we invert the magnetic field direction. This effect is partially resolved at about 2σ.

We believe that the most likely cause of this effect is a small, HV-correlated motion of the Hg vapor cells. We would expect such motion to be independent of the direction of $\mathbf{B}$. Since the magnetic field is not perfectly uniform, any cell motion could produce a shift in the Larmor frequencies, and hence a shift in the combo channel ν_c. If the main magnetic field reverses perfectly, a consistent HV-correlated movement of the vapor cells would have the same effect for the two $\mathbf{B}$ directions, thus adding a B-even offset to the measurement.

In addition, analysis shows that the outer top (OT) and middle top (MT) cells contribute significantly more to this effect than the bottom two cells. If this is the case,

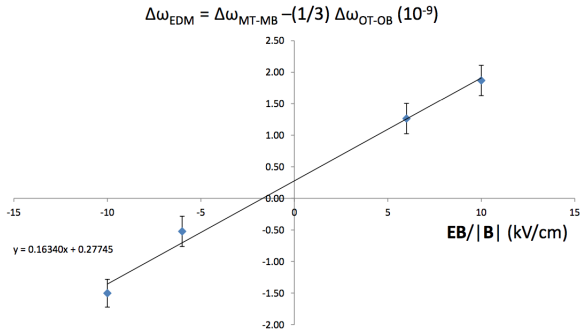

FIG. 3. The frequency shift $\Delta\omega_{\rm EDM} = 2\pi\Delta\nu_c$ in the combo (EDM) channel (units of 10^{-9} rad/s) plotted for four field configurations (combinations of **B** up or down and $E = 6$ or 10 kV/cm). We refer to the nonzero y-intercept as the "B-even effect." Credit: Brent Graner.

then we would expect to see that the top cells experience stronger magnetic field gradients than the other two cells.

B. Outer Cells Frequency Difference

We also observe a HV-correlated frequency difference between the outer top (OT) and outer bottom (OB) cells. Recall that the outer cells experience $E = 0$, so any HV-correlated frequency difference between the OT and OB cells is indicative of a systematic effect that can feed through to our EDM signal. This frequency difference is partially resolved at about 2σ, and is much larger in runs that are cut from the EDM dataset (about 8.7σ). We refer to this effect as the "OT–OB" systematic.

We believe that this systematic is most likely caused by the same mechanism as the B-even effect. Suppose that the outer cells difference is caused by HV-correlated cell motion in a non-uniform magnetic field. This effect can be decomposed into a part that reverses with the magnetic field and a part that does not. The former would appear as a as a B-even offset to the data, while the latter would appear as a HV-correlated and B-odd outer cell difference.

An HV-correlated and B-odd frequency shift in the EDM channel mimics an EDM, so it is important to bound the feed through of the B-odd OT–OB systematic to the EDM measurement. Assuming that the outer cells systematic is caused by cell motion, the effect can be directly simulated by translating the cells and measuring the ratio of the change in the combo channel frequency to the change in the outer cells frequency difference.

IV. MAGNETIC FIELD MAPPING

The two systematic effects discussed above can be directly investigated by mapping the magnetic field gradients inside of the apparatus.

With no applied electric field, all four Hg vapor cells act as magnetometers with no EDM sensitivity. Then, the most direct way to measure magnetic field gradients is by translating the vapor cells, taking Larmor frequency measurements for each cell at each position. In this manner, we have completed field mappings by translating the cells in the $\hat{x}$ (horizontal), $\hat{y}$ (vertical), and $\hat{z}$ (magnet coil axis) directions. Fig. 4 depicts the coordinate system.

To replicate the field inside of the apparatus during actual data runs, all three layers of magnetic shielding must be closed while taking the field mapping. However, access to the inside of the main magnet coil is very limited when the magnetic shields are closed, aside from the holes in the shields that provide optical access to the vessel. These holes lie along $\hat{x}$ for the middle two cells, and along $\hat{z}$ for the outer two cells. In addition, the shields cannot be opened to allow access for translating the vessel during a measurement, since the field inside of the apparatus changes by a small but significant amount each time the shields are opened, closed again, and degaussed. Finally, any new parts placed inside of the magnetic shields must be made of a non-magnetic material, such as plastic. To address these specifications, three translation apparatuses were built for moving the vessel in each direction.

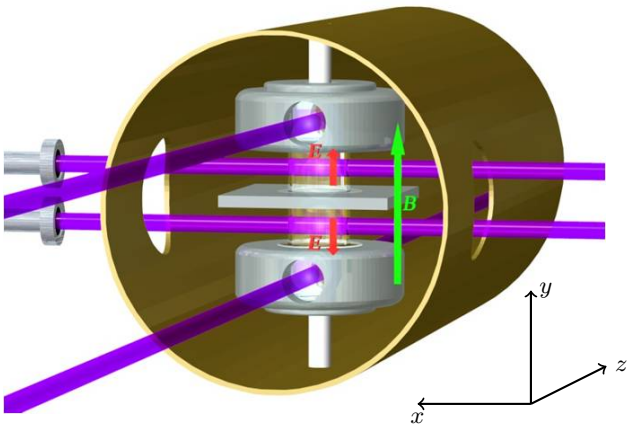

FIG. 4. Coordinate system for the experiment, showing $\hat{x}$ (transverse), $\hat{y}$ (vertical), and $\hat{z}$ (coil) axes. Original image from Ref. [4].

We primarily consider the frequency differences between the cells to cancel common-mode noise such as low frequency drift. This was necessary since it typically took several minutes to realign optics after each time the vessel was translated. In addition, our data analysis program uses frequency differences between cells in its calculations, since most quantities of interest (e.g., the combo and OT–OB channels) are expressed as differences in cell frequencies. Therefore, it was convenient to work primarily with the frequency differences between cells rather than individual cell frequencies.

A. Mapping along $\hat{x}$

The translation apparatus for the $\hat{x}$ direction consisted of a platform to support the vessel, with a shape adapter (ring used to secure the vessel in the magnet coil) attached to each end. A square piece of plastic was machined to replace the bottom HV feedthrough on the vessel. Finally, a pocket was milled into the platform which allows the square piece to slide along the $\hat{x}$ direction. When the square piece is screwed into the bottom of the vessel, the vessel is able to translate smoothly along $\hat{x}$ for 2.5 mm in either direction, without twisting about the vertical axis ($\hat{y}$) or moving along the coil axis ($\hat{z}$). Thin strings were tied to the vessel and threaded through the holes in the shields that run along $\hat{x}$, and were used to pull the vessel between the center and $x = \pm 2.5$ mm positions. Fig. 5 shows the $\hat{x}/\hat{z}$ translation apparatus compared to the setup used for EDM measurements.

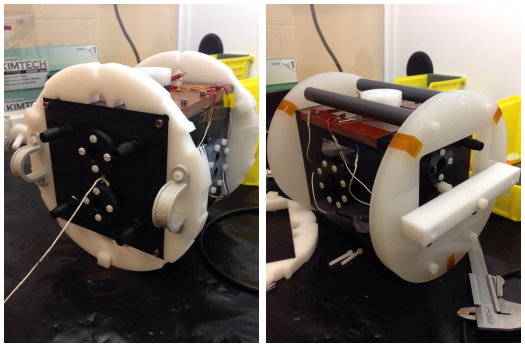

FIG. 5. Left: The EDM vessel with original shape adapters attached. This setup is used while taking EDM data, and was also used for some of the $\hat{z}$ translation data.
Right: The EDM vessel in the $\hat{z}$ translation apparatus. The $\hat{x}$ translation apparatus is identical in appearance.

To produce the magnetic field mapping, the vessel was first centered in the $\hat{x}$ direction with the magnetic shields open. The dB_y/dx gradient coil was set to a typical value for normal EDM measurements. The shields were closed and degaussed, and the two linear dB_y/dy gradient coils and laminate (main magnet coil endcap) gradient coil were calibrated; this is the standard procedure for cancelling gradients in the $\hat{y}$ direction, and these gradient coils are reset daily while taking EDM data. Frequencies of all four cells in the center position were measured. Then, the vessel was translated to $x = +2.5$ mm (then $x = -2.5$ mm) and the measurement was repeated.

Fig. 6 shows the field mapping. The left subplot shows the field mapping obtained with **B** pointing up ($+\hat{y}$), while the right subplot shows **B** pointing down ($-\hat{y}$). Each subplot was created from the average of two measurements, with the magnetic shields degaussed after each individual measurement. The plots were colored on the same symmetric logarithmic color scale to make the overall field pattern more apparent.

The data show that the magnetic field gradients in the

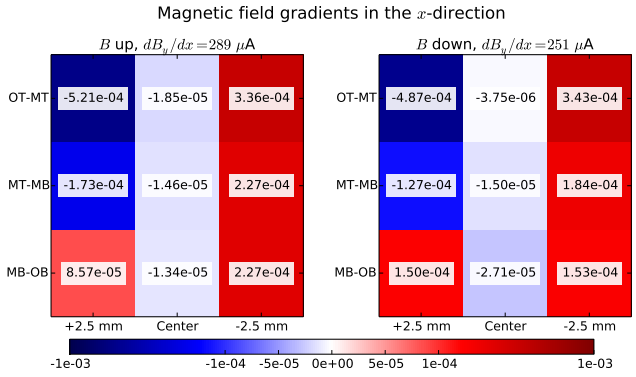

FIG. 6. Field mapping obtained by translating the vessel ± 2.5 mm in the $\hat{x}$ direction. Values on the plot are cell differences in units of rad/s. Both subplots were colored on the same symmetric logarithmic color scale using `matplotlib`.

$\hat{x}$ direction reverse fairly well when the overall field is reversed. In addition, the outer top (OT) cell appears to experience the strongest gradients; we expect this to be the case, since OT cell has the largest contribution to the B-even systematic.

Letting ν_{34}^{+} (ν_{34}^{-}) denote the frequency difference between the outer top and outer bottom cells in the $+(-)2.5$ mm position, and applying the approximation that the field gradients are linear, we can approximate the magnitude of the gradient as

$$\left| \frac{1}{\gamma} \frac{\nu_{34}^{+} - \nu_{34}^{-}}{d} \right| \approx 0.5 \ \mu\text{G cm}^{-1}, \tag{4}$$

where $\gamma \approx 771$ Hz/G is the gyromagnetic ratio of ^{199}Hg [5], and $d = 0.5$ cm is the distance between the two measurement positions. Given this gradient, cell motion of ~ 10 nm is enough to cause the angular frequency differences that appear in the EDM dataset, which are on the order of $\sim 10^{-10}$ rad/s.

B. Mapping along $\hat{z}$

The translation apparatus for the $\hat{z}$ direction was similar to the one made for the $\hat{x}$ direction, except that the pocket in the platform was rotated 90° to allow the vessel to slide along the $\hat{z}$ axis.

The $\hat{z}$ mapping was taken using the same procedure as the $\hat{x}$ mapping. The vessel was first centered in the $\hat{z}$ direction with the magnetic shields open. The dB_y/dx gradient coil was set to a typical value for normal EDM measurements. The shields were closed and degaussed, and the gradient coils were calibrated. Frequency measurements for all four cells in the center position were performed. Then, the vessel was translated to $z = +2.5$ mm (then $z = -2.5$ mm) and the measurement was repeated. Fig. 7 displays this data, plotted on the same symmetric logarithmic color scale as Fig. 6.

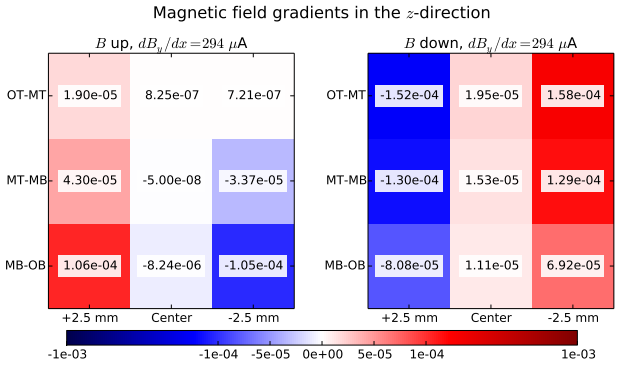

FIG. 7. Field mapping obtained by using the new translation apparatus to translate the vessel ±2.5 mm in the $\hat{z}$ direction. Values on the plot are cell differences in units of rad/s. Subplots were colored on the symmetric logarithmic color scale used in Fig. 6 for comparison.

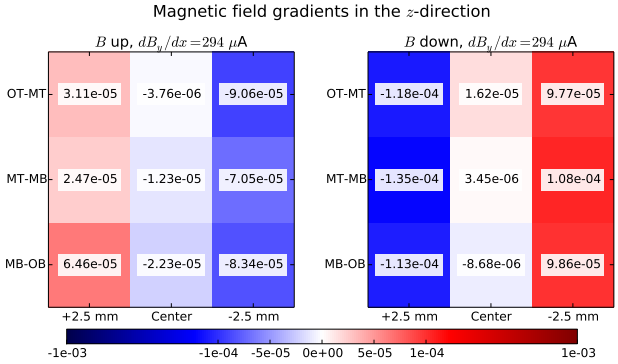

FIG. 8. Field mapping obtained by pushing and pulling the old shape adapters to translate the vessel ∼ ±2.5 mm in the $\hat{z}$ direction. Values on the plot are cell differences in units of rad/s. Subplots were colored on the symmetric logarithmic color scale used in Fig. 6 for comparison.

The same measurements were also taken with the original shape adapters attached to the vessel; the entire vessel and shape adapters assembly was translated approximately +(−)2.5 mm from the center position by pushing (pulling) on the vessel with a rod (string) inserted through the holes in the magnetic shields. Data taken using this measurement technique is shown in Fig. 8. By comparing Figs. 7 and 8, one can see that data taken using the two measurement techniques mostly coincide. We believe that the observed differences are due to small inconsistencies in the amount the vessel was translated in the second method.

Note that the gradients in the $\hat{z}$ direction are comparable, but slightly smaller than those in the $\hat{x}$ direction. Repeating the calculation from Eq. 4 for the $\hat{z}$ data yields $\approx 0.1\ \mu\text{G cm}^{-1}$, so the $\hat{z}$-gradients appear to be about a factor of 5 smaller than the $\hat{x}$-gradients.

In addition, Figs. 7 and 8 show that the $\hat{z}$-gradients do not reverse completely upon flipping the magnetic field – indeed, the fields look much different between the **B** up and **B** down plots. We believe that this effect is due to our magnetic shields, which may not be perfectly symmetric with respect to the two **B** directions. This indicates that cell motion in the $\hat{z}$ direction should result in a large B-odd OT–OB effect.

C. Mapping along $\hat{y}$

The translation apparatus for the $\hat{y}$ direction utilized an improvised air bladder to translate the vapor cells. Specifically, two identical rectangular plastic plates were used to support the cells. One of the plates was stationary and screwed into the shape adapters to act as a base. The second plate was positioned on top of the first, and holes were drilled to insert long screws pointing vertically. These screws acted as rails to restrict the motion of the upper plate to the $\pm\hat{y}$ direction. Stops were attached to the rails to allow the plate a 2 mm range of movement. Finally, inflatable tubing was inserted between the plates to provide the gentle force necessary to lift the upper plate. The vapor cells were removed from the vessel and attached to the top of the upper plate in a stack. The plates were designed such that, when the tubing is deflated, the vapor cells sit 1 mm below their usual position for EDM data; when the tubing is completely inflated, the cells sit 1 mm above their usual position. The translation apparatus is shown in Fig. 9.

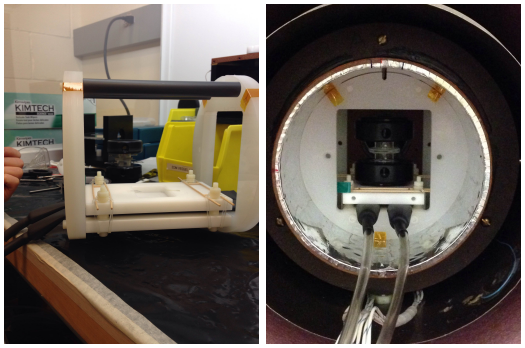

FIG. 9. Left: The $\hat{y}$ translation stage before the cells have been attached. Right: The stage with vapor cells attached, partially inserted into the main magnet coil.

A single measurement consists of degaussing the magnetic shields and setting the gradient coils with the cells in the lowered position. Larmor frequencies are measured with the cells in both the lowered position and raised position. It is not clear that the two linear dB_y/dy gradient coils and the laminate coil produce the same magnetic field gradients when they are calibrated with the cells in the raised (+1 mm) and lowered (−1 mm) positions, so the gradient coils are set with the cells in the raised position frequency measurements are taken for the raised and lowered positions. These two pairs of measurements

are then averaged together to obtain a measurement of the gradients in the $\hat{y}$ direction.

	OT−MT	MT−MB	MB−OB	OT−OB
B up	3.28	−1.72	3.31	4.88
B down	3.38	−1.72	3.40	5.06

FIG. 10. Field mapping obtained by translating the cells 2 mm in the $\hat{y}$ direction. The values in the table are frequency differences in units of 10^{-4} rad/s. The OT–MT value in the table was obtained by finding the frequency differences $\Delta\nu_{31} = \nu_{\rm OT} - \nu_{\rm MT}$ for the raised and lowered positions and taking their difference $(\Delta\nu_{31}^{\rm raised} - \Delta\nu_{31}^{\rm lowered})$; similarly for the other cell differences.

The results are summarized in Fig. 10. Each row of data in the table consists of the average of four of the measurements described in the previous paragraph. The field appears very similar between the two field configurations, which indicates that the field gradients in the $\hat{y}$ direction reverse to a large extent when the main magnetic field is reversed.

D. Discussion

We are primarily interested in the feed through of the outer cells difference $\nu_{34} = \nu_{\rm OT} - \nu_{\rm OB}$ to the combo (EDM) channel, $\nu_c = \nu_{\rm MT} - \nu_{\rm MB} - \frac{1}{3}(\nu_{\rm OT} - \nu_{\rm OB})$.

For concreteness, we consider the $\hat{x}$ direction in detail, although the same calculations apply to the $\hat{y}$ and $\hat{z}$ data. For a given field direction, let $\Delta\nu_\alpha$ be the average of the measured differences $\nu_\alpha(+x) - \nu_\alpha(-x)$, where $\alpha \in \{c, 34\}$ denotes the frequency combination in question. Then, we can compile a table of the values of $\Delta\nu_{34}$, $\Delta\nu_c$, and the feed through $R = \Delta\nu_c/\Delta\nu_{34}$ for each $\mathbf{B}$ direction, as shown in Fig. 11.

$\hat{\boldsymbol{x}}$	$\Delta\nu_{34}$ (rad/s)	$\Delta\nu_c$ (rad/s)	R
B Up	-1.40×10^{-3}	6.59×10^{-5}	-4.71×10^{-2}
B Down	-1.14×10^{-3}	7.02×10^{-5}	-6.13×10^{-2}

FIG. 11. Comparison of the $\hat{x}$-gradient data between the two magnetic field directions. Here $R = \Delta\nu_c/\Delta\nu_{34}$.

Approximating the difference in the signal between the two magnetic field directions as linear, we can separate the frequency differences $\Delta\nu_\alpha$ into a B-even and B-odd part,

$$\Delta\nu_\alpha(\uparrow / \downarrow) = \left(\frac{\Delta\nu_\alpha(\uparrow) + \Delta\nu_\alpha(\downarrow)}{2}\right) \pm \left(\frac{\Delta\nu_\alpha(\uparrow) - \Delta\nu_\alpha(\downarrow)}{2}\right), \tag{5}$$

where the first term in Eq. 5 represents the B-even portion of the signal and the second term represents the B-odd portion of the signal. Thus, we can rewrite the table in Fig. 11 in terms of the B-even and B-odd parts, as shown in Fig. 12.

$\hat{\boldsymbol{x}}$	$\Delta\nu_{34}$ (rad/s)	$\Delta\nu_c$ (rad/s)	R
Even	-1.27×10^{-3}	6.80×10^{-5}	-5.35×10^{-2}
Odd	-1.27×10^{-4}	-2.14×10^{-6}	1.69×10^{-2}

FIG. 12. Comparison of the B-even and B-odd parts of the $\hat{x}$-gradient data.

The quantity $R_{\rm even} = -5.35\%$ is the B-even feed through of the outer cells difference to the combo (EDM) channel. This value is an estimate of how an outer cell difference caused by motion in the $\hat{x}$ direction would feed through to the B-even systematic. Similarly, the quantity $R_{\rm odd} = 1.69\%$ is the B-odd feed through of the outer cells difference to the combo channel. Since this signal is odd with respect to the magnetic field direction, it mimics an EDM, so this quantity is an estimate of the effect of the OT–OB systematic on our EDM measurement. By repeating this measurement several times, we can reduce our uncertainty in the values of $R_{\rm even}$ and $R_{\rm odd}$, which should help us place an upper bound on the feed through of the B-even and B-odd effects caused by cell movement in the $\hat{x}$ direction.

$\hat{\boldsymbol{x}}$	$\Delta\nu_{34}$ (rad/s)	$\Delta\nu_c$ (rad/s)	R
Even	-1.27×10^{-3}	6.80×10^{-5}	-5.35×10^{-2}
Odd	-1.27×10^{-4}	-2.14×10^{-6}	1.69×10^{-2}
$\hat{\boldsymbol{y}}$	$\Delta\nu_{34}$ (rad/s)	$\Delta\nu_c$ (rad/s)	R
Even	5.07×10^{-4}	-3.42×10^{-4}	-6.75×10^{-1}
Odd	-1.90×10^{-5}	7.70×10^{-6}	-4.06×10^{-1}
$\hat{\boldsymbol{z}}$	$\Delta\nu_{34}$ (rad/s)	$\Delta\nu_c$ (rad/s)	R
Even	-1.66×10^{-4}	-2.22×10^{-5}	1.34×10^{-1}
Odd	5.39×10^{-4}	-4.34×10^{-6}	-8.05×10^{-3}

FIG. 13. Compilation of the B-odd and B-even parts of three sets of cell translation data.

Similar calculations for the $\hat{y}$ and $\hat{z}$ measurements have been performed. Data for all three directions is summarized in Fig. 13. Note that in the $\hat{z}$ direction, the odd portion of $\Delta\nu_{34}$ is actually larger than the even portion. This is consistent with the actual EDM dataset, where the B-odd portion of the OT–OB systematic is larger than the B-even portion. For this reason, we suspect that cell motion in the $\hat{z}$ direction may explain the OT–OB systematic. The cables that supply the HV to the vessel run along the $\hat{z}$ direction; polarity-dependent tension in these cables provides a possible mechanism for cell movement in the $\hat{z}$ direction.

V. NEW MAGNETIC SHIELD

A more uniform magnetic field inside of the apparatus would be a significant improvement to the experiment, since it would markedly suppress systematic errors due to

magnetic field gradients. Imperfections in the magnetic shields, such as dents and welds, can cause magnetic field gradients. We plan to add a new, innermost magnetic shield for the next generation of the experiment. The new shield should be constructed as uniformly as possible, which means no welds or dents should be present. To achieve this, we plan to construct the shield out of four layers of 0.002"-thick high permeability mu-metal foil, wrapped on a linen-grade phenolic tube base.

Several strategies for winding magnetic shields are given in Ref. [6]. However, all of these windings contain many seams, which may negatively affect the uniformity of the shield. For this reason, any winding scheme employed will likely prioritize minimizing the seams in the middle of the shield to maximize field uniformity near the vessel.

The three magnetic fields currently in the apparatus provide a transverse shielding factor of $S_{\text{old}} = 5 \times 10^4$ [3]. The shielding factor due to multiple shields can be calculated using the following expression,

$$\begin{aligned} S = 1 &+ \sum_{i=1}^{n} S_i + \sum_{i=1}^{n-1}\sum_{j>1}^{n} S_i S_j \left(1 - \frac{R_i^2}{R_j^2}\right) \\ &+ \sum_{i=1}^{n-2}\sum_{j>i}^{n-1}\sum_{k>j}^{n} S_i S_j S_k \left(1 - \frac{R_j^2}{R_k^2}\right)\left(1 - \frac{R_i^2}{R_j^2}\right) \\ &+ \cdots \\ &+ S_n \prod_{i=1}^{n-1} S_i \left(1 - \frac{R_i^2}{R_i + 1^2}\right), \end{aligned} \tag{6}$$

where $S_i = \mu_i t_i / 2R_i$, μ_i is the relative permeability of the ith shield, t_i is the thickness of the ith shield, R_i is the average radius of the ith shield, and the index runs from the innermost ($i = 1$) to outermost shield [7]. Using this expression and the known radii $R_i = \{6'', 9'', 12''\}$ and thickness ($t = 0.03''$) of the current shields, we estimate the mu-metal used in the shields has relative permeability $\mu = 32,610$. This is in good agreement with the advertised value of μ for the mu-metal sheets.

Using this information and Eq. 6, we can calculate the increase in the shielding factor upon adding the new shield. Using the known dimensions $R = 5.5''$ and $t = 0.008''$ for the shield, and a reasonable estimate of $\mu = 30,000$ for the mu-metal foil, we obtain a transverse shielding factor of $S_{\text{new}} \sim 235,000$, nearly a factor of 5 improvement over the old shielding factor.

VI. SUMMARY

We have completed preliminary mappings of the magnetic field gradients in the $\hat{x}$, $\hat{y}$, and $\hat{z}$ directions. These measurements can help to explain the dominant systematics effects in the latest EDM dataset, and repeating these measurements will allow us to place an upper bound on the feed through of these systematics to our EDM measurement. To improve the magnetic field uniformity, we plan to add a new magnetic shield made out of thin mu-metal foil. We expect that the new shield will also increase our transverse shielding by a factor of 5.

ACKNOWLEDGMENTS

I would like to thank Blayne Heckel, Jennie Chen, Brent Graner, Eric Lindahl for their excellent guidance, and for generously sharing their time and knowledge with me this summer. I am very grateful to Ron Musgrave for his invaluable help in the machine shop. Many thanks to Deep Gupta, Alejandro Garcia, Gray Rybka, Shih-Chieh Hsu, Linda Vilett, and Farha Habib for organizing a wonderful program this summer. Finally, thank you to the INT REU Program and the NSF for this opportunity, and thanks to the other REU students – it was fun hanging out!

[1] J. Ginges and V. Flambaum, Physics Reports **397**, 63154 (2004).
[2] W. C. Griffith, M. D. Swallows, T. H. Loftus, M. V. Romalis, B. R. Heckel, and E. N. Fortson, Phys. Rev. Lett. **102**, 101601 (2009).
[3] M. D. Swallows, T. H. Loftus, W. C. Griffith, B. R. Heckel, and E. N. Fortson, Phys. Rev. A **87**, 012102 (2013).
[4] W. C. Griffith, PhD thesis, Univ. of Washington (2005).
[5] M. D. Swallows, PhD thesis, Univ. of Washington (2007).
[6] Susan K. Malkowski, Master's thesis, University of Kentucky, 2011.
[7] T.J. Sumner, J.M. Pendlebury, and K.F. Smith, J. Phys. D: Appl. Phys. 20, 1095 (1987).